FROM: ADVANCED EPR. APPLICATIONS IN BIOLOGY AND BIOCHEMISTRY
A.J. Hoff, Ed., Elsevier, Amsterdam, 1989, CHAPTER 8, pp. 307-340.

ELECTRON PARAMAGNETIC RESONANCE AT 1 MILLIMETER WAVELENGTHS

DAVID E. BUDIL, KEITH A. EARLE, W. BRYAN LYNCH, AND JACK H. FREED

1. INTRODUCTION

For over two decades, new technical developments in EPR spectroscopy have lagged behind analogous advances in the field of NMR. Techniques such as Fourier-transform and two-dimensional correlation spectroscopy, which have long been standard in NMR, have only relatively recently found application in EPR (1). One of the most important advances in NMR has been the extension to high frequencies, requiring the use of superconducting magnets. This has provided large enhancements in sensitivity and spectral resolution, greatly broadening the utility of NMR techniques, especially for biological applications (2).

Recent years have witnessed a similar trend in EPR spectroscopy. The effort towards higher EPR fields and frequencies has in large part been fostered by an emerging technology in the synthesis and processing of signals in the far-infrared (FIR) and millimeter wave regions (3) for applications in radar, communication, and radioastronomy. Notable in the field of EPR has been the development and application of a spectrometer working at λ = 2 mm (i.e. 148 GHz) and 5.3 Tesla fields by Lebedev and co-workers (4). They have reported EPR spectra of nitroxide spin labels in liquid and solid phases, emphasizing the significant advantages of high resolution for determining g-tensors and studying molecular dynamics in the slow-motional regime (5). The sensitivity at 148 GHz is also reported to be significantly better than that of conventional EPR spectrometers. More recently Möbius has constructed an EPR spectrometer operating at λ = 3.2 mm (94 GHz) in a 3.4 T field with similar advantages (6).

Theoretically, even greater enhancements in sensitivity should be realized at still higher frequencies. However, there are two major technical obstacles to extending the frequency range for practical EPR work. First, high resolution EPR at high frequencies would require magnets that can provide very high fields with a homogeneity as good as $1:10^6$. Although EPR has been performed in pulsed magnetic fields of up to 35 T (7), persistent fields with sufficient homogeneity for high resolution EPR work are currently only available up to about 15 T (8). Second, it becomes increasingly difficult to utilize standard microwave technology at higher frequencies, even though this has proved possible at λ = 2 to 3 mm. Waveguides, cavities, and other components are exceedingly small and lossy, and are often quite difficult to fabricate for shorter wavelengths.

A comfortable compromise is presently accessible at fields of 8-12 T, corresponding to wavelengths of 1.0 - 1.5 mm (200-300 GHz), where superconducting magnets with good homogeneity can be manufactured with relative ease. Even at these wavelengths, however, conventional microwave technologies are no longer adequate. In this chapter we describe a new EPR spectrometer operating at λ = 1.2 mm (250 GHz) in a field of 9 T that takes advantage of far-infrared technology based upon the principles of Gaussian optics (9). Such quasi-optical techniques greatly simplify the design and performance of the high-frequency EPR spectrometer, and they appear to be the natural way to proceed with submillimeter EPR spectroscopy in the future.

After describing our new design, we present a selection of experiments which illustrate the potential utility of FIR-EPR, particularly with respect to studies of motional dynamics and biologically relevant spin labels. We then discuss currently available components and technology that will make possible future improvements and refinements of EPR spectroscopy at millimeter and sub-millimeter wavelengths.

2. THE 1 MILLIMETER SPECTROMETER

2.1 Overview

Our 1.20 mm EPR spectrometer operates at 249.9 GHz and 8.9 T for g = 2. The basic design is a simple transmission cavity configuration, shown schematically in Fig. 1. The cavity is comprised of two mirrors, each of which is attached to a tube that serves as a beam guide for the 1 mm waves. The 1 mm beam travels from the source, located underneath the magnet, through a series of lenses to the cavity, and then through a second series of lenses to a detector which is mounted on top of the magnet Dewar. Since the source delivers only 5 mW of power, optimal alignment of the cavity mirrors and the lenses between source, cavity, and detector is crucial to a successful experiment.

The spectrometer is quite easy to operate; in fact, its operation is in a number of ways very similar to a conventional 9 GHz EPR spectrometer once the main magnet coil is driven up to a field value near resonance. The resonance is found by sweeping the sweep coil. The maximum sweep rate of 3.5 mT/second is quite adequate when compared to a 9 GHz EPR spectrometer, and permits easy initial location of the resonance signal.

From the experimental high-field spectra we have obtained, we estimate a minimum number of observable spins as low as 3×10^{11} spins for a 0.1 mT linewidth with no source attenuation (3.5 mW of incident power), 80 kHz field modulation, and a lock-in amplifier bandwidth of 0.1 Hz. For our resonator and sample holder, this would correspond to a minimum detectable molarity, M_{min} of 8×10^{-9} M in a low-loss solvent. Such a sensitivity is quite comparable to that of a 9 GHz EPR spectrometer for narrow-line spectra.

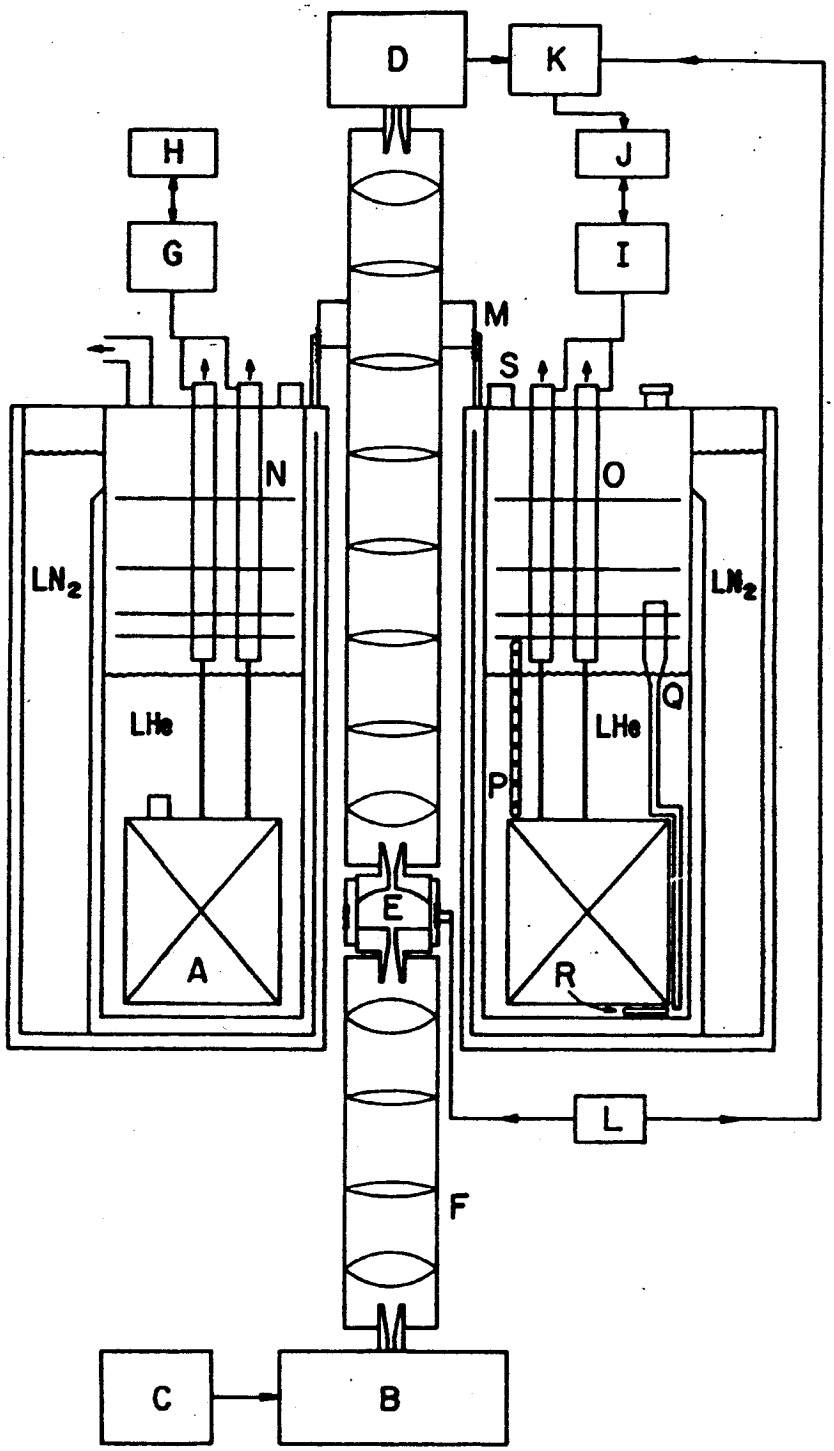

Fig. 1. Block diagram of 249.9 GHz EPR spectrometer. A: 9 T Superconducting solenoid and 57.0 mT sweep coils. B: Phase-locked 250 GHz source. C: 100 MHz reference oscillator. D: Schottky diode detector. E: Semiconfocal Fabry-Perot cavity and field modulation coils. F: 250 GHz quasi-optical beam guide. G: Main coil power supply (100 A). H: Main coil current programmer. I: Sweep coil power supply (50 A). J: Personal computer. K: Lock-in amplifier. L: Field modulation and lock-in reference oscillator. M: Cavity tuning screw. N: Vapor-cooled leads for main solenoid (non-retractable). O. Vapor-cooled leads for sweep coil (non-retractable). P: LHe level indicator. Q: LHe transfer tube. R. Bath temperature and heater resistors. S: LHe blow-off valves. [From Ref. 9].

2.2 Magnet system

The superconducting magnet was built by American Magnetics, Inc. (AMI) and has a maximum field value of 9.2 T at 4.2 K, corresponding to a current of about 72 amps. In addition to the main 9.2 T coil, the magnet has an auxiliary superconducting field-sweep coil, which can be swept ±54.0 mT (38 amps) while the main coil is persistent, making the spectrometer similar in field operation to a conventional EPR spectrometer. The sweep coil is designed to minimize mutual inductance with the main coil, which permits rapid field sweeps without significant interference with the main coil. The magnet measures 33.5 cm in length with an outer diameter of 19.1 cm, and a bore diameter of 6.1 cm. Field homogeneity within a central 1 cm diameter spherical volume is better than 3×10^{-6} without shims for all values of the sweep coil current, and the field is persistent at 9 T to at least 10^{-7}/hour.

The leads supplying current to both main and sweep coils are non-retractable. The main magnet coil is charged by a Hewlett-Packard (HP) 6260B DC power supply which is controlled by an AMI 402A programmer. An HP 6032A DC power supply with a GPIB interface to a PC drives the sweep coil, providing accurate and reproducible field sweeps. The programmable voltage limit of the sweep power supply prevents the buildup of inductive voltage across the sweep coil that would otherwise quench the magnet during fast sweeps. This feature permits a maximum sweep rate of about 3.5 mT/second in either direction, which is useful for initial location of signals or pre-setting the spectrometer to a spectral region of interest. However, the inductive load compensation circuitry of the power supply produces considerable hysteresis at such high sweep rates; to avoid systematic deviations in spectral line positions with respect to the direction or rate of field sweep, the magnet must be swept at 0.03 mT/second or less. Under such conditions, the sweep is reproducible to within the programming resolution of the power supply, or about 19 μT. Reproducibility between runs (that is, after cycling the sweep power supply over a wide range or turning it off) is limited by the programming accuracy of the power supply, and is usually better than 0.1 mT, or 1 part in 10^5 of the applied field. Accurate calibration of the sweep coil was made using the known hyperfine splitting of PDT in decane (10).

The Dewar containing the magnet is a liquid nitrogen (LN_2) jacketed warm bore design built by Cryofab, Inc. according to our own specifications. The bore has inner and outer diameters of 4.4 cm and 5.7 cm respectively; the liquid helium (LHe) chamber is 21.6 cm in diameter and 122 cm long. An AMI LHe level detector monitors the liquid level above the magnet. A series of copper baffles reduces the LHe evaporation rate of the empty dewar to about 0.4 ℓ/hr. Boil off caused by the main and sweep coil current leads is minimized by using a design similar to that of Efferson (11). Each lead consists of several brass ribbons (each ribbon is 0.1 mm thick, 6 mm wide and 46 cm long) contained within a fiberglass

tube that maintains a flow of cold escaping He vapor over them. The main magnet leads contain 40 ribbons each and are capable of carrying 100 amps; the sweep coil leads can carry 50 amps with 24 ribbons each.

With the magnet and leads in place, the maximum LHe boil off rate is less than 0.75 ℓ/hr. Since our dewar holds 12 ℓ of liquid above the magnet, the time available for experiments between LHe transfers is about 15 hours, which is more than enough time to perform most experiments. All helium gas is collected for reliquefaction. A LHe transfer line extension inside the dewar allows us to transfer liquid efficiently to the bottom of the dewar, where a carbon resistor monitors the temperature during the initial cool down.

2.3 Millimeter wave source

Our 1 mm wave source is a Millitech Corp. PLS-3F phase locked solid state source which delivers 5 mW at 249.9 GHz (WR-4 waveguide). The self-locking feature of the source makes it very easy to operate and provides a much less noisy output than other sources of radiation in the 1 mm wavelength region. It is much smaller than an FIR laser system (which can produce 1.222 mm waves), and it does not have the problems of stability and maintenance inherent to a laser (12).

Fig. 2 shows a schematic diagram of the control loop. The heart of the source is a InP Gunn oscillator (Millitech GDM-10T) that is phase locked to a highly stable oven-controlled 100 MHz crystal oscillator (Vectron CO224A59) reference. The Gunn output (40 mW) is locked to 83.3 GHz and then converted to 249.9 GHz using a tripler based on a GaAs diode (13) (Millitech MU3-04T). We estimate (14) that the phase noise is -80 dBc/Hz with respect to 83.3 GHz, and -70 dBc/Hz with respect to 249.9 GHz at an offset frequency of 10 kHz. (At a 100 kHz offset, these figures are approximately -100 dBc/Hz and -90 dBc/Hz at 83.3 GHz and 249.9 GHz, respectively.) The output frequency can be swept within a ±65 MHz range by sweeping the reference ±25 kHz. Although the output power is not variable, the power incident on the cavity may be attenuated as needed by inserting calibrated FIR attenuators (made from e.g. carbon black) into the FIR beam.

2.4 Transmission of 1 millimeter waves

Low-loss quasi-optical techniques (15) are used to propagate the millimeter wave beam from the source into the warm bore of the Dewar to the cavity and then on to the detector. Feedhorns "launch" the linearly polarized beam from a waveguide mode to a free space TEM_{00} mode that can be propagated through a series of lenses. An adequate approximate solution to the wave equation for such a free space mode has a gaussian distribution of the E and H field amplitudes transverse to the direction of propagation.

In our system (cf. Fig. 1) a Millitech scalar feedhorn converts the waveguide mode into a gaussian beam as it exits the source. The base of the feedhorn

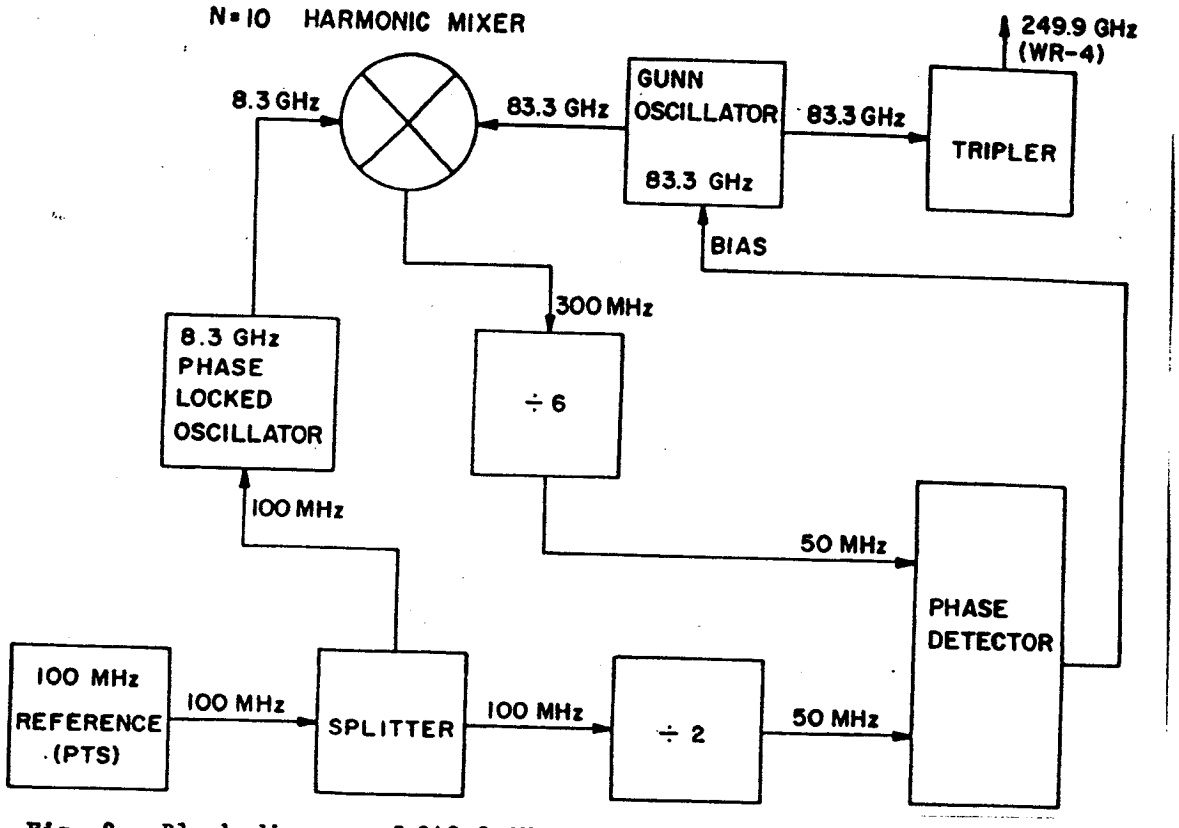

Fig. 2. Block diagram of 249.9 GHz source. [From Ref. 9].

contains a rectangular to circular waveguide transition, so that it may be directly coupled to the source waveguide. The diverging gaussian beam passes through a focusing lens (diameter 2.3 cm, focal length 2.75 cm) and is focussed to a beam waist of radius 1.6 mm. Subsequently a series of longer focal length primary lenses (diameter 3.51 cm, focal length 11.4 cm, beam waist radius 6.6 mm) are used to propagate the beam over longer distances. Both focusing and primary lenses are made of teflon and have anti-reflection surface grooves designed to match the refractive indices of teflon and air at 249.9 GHz (16).

Radiation is coupled into and out of the cavity by using two conical feedhorn/focusing lens pairs. The aperture diameter D of each feedhorn was adjusted to couple to the beam waist radius of the focusing lens, w_0, according to the relationship $D = 3w_0$, which is valid for low aperture phase error scalar horns (15). Another conical feedhorn (from Custom Microwave)/focusing lens pair couples radiation from the TEM_{00} mode back to a short length of WR-4 rectangular waveguide in front of the detector. Because the FIR radiation maintains its linear polarization during its traverse of the magnet bore, the rectangular waveguide at the detector must be properly aligned relative to the source waveguide for optimal coupling into the detector. Alignment of source and detector waveguides also ensures that the observed EPR signal is in phase (i.e.,

a pure absorption signal); misalignment of the detector results in a small admixture of dispersion in the EPR spectrum.

This quasi-optical approach provides much more efficient transmission and coupling of 1.2 mm radiation than would conventional waveguide techniques. The loss due to the lenses over a 1.4 m path length is only 2 dB, whereas the theoretical loss of WR-4 waveguide over the same distance is 16 dB. In addition, the gaussian beam is easily coupled into useful waveguide or cavity modes. The conical antennae used in our system are readily fabricated, and do not produce severe losses with gaussian beams. The scalar feedhorn reduces coupling losses even further: its radiation pattern has much smaller side lobes than that of the conical antennae, so that it more closely matches the shape of the fundamental mode of the gaussian beam.

2.5 EPR cavity

The cavity (Fig. 3) is a semi-confocal Fabry-Perot resonator having 2.5 cm diameter mirrors. The radius of curvature of the spherical mirror is also 2.5 cm; thus, the optimum inter-mirror distance for propagating the fundamental mode is one-half the radius of curvature, or 1.25 cm. This corresponds to a mode number, ν = 20 (i.e. the number of half wavelengths between the mirrors). The cavity is coupled to two locally made feedhorns by 1.5 mm diameter coupling holes located at the center of each mirror. To tune the cavity, transmitted power is maximized by raising and lowering the spherical mirror with respect to the flat mirror. The spherical mirror and upper optical guide are translated (and rotated) by a locally made millimeter screw located at the top of the dewar with a vertical travel of 0.635 mm/turn. The spherical mirror slides within a teflon sleeve that is affixed to the lower flat mirror. To measure transmitted 1.20 mm power, we use phase sensitive detection referenced to a homemade (nonmagnetic) beam chopper that operates at 100 Hz. Fig. 4 shows the series of resonances in transmitted power that are observed as a function of mirror translation.

Some performance characteristics of the cavity are apparent from Fig. 4. In addition to the intense, regularly spaced resonance peaks of the $TEM_{00\nu}$ cavity mode, other less intense peaks corresponding to different cavity modes are observed, often as shoulders of the main peaks. As the lower trace of Fig. 4 shows, the introduction of even low-loss hydrocarbon solvents into the cavity increases such mode conversion and thus cavity losses.

The loaded Q of the cavity, Q_L, is easily determined from Fig. 4 for a given tuning peak. The cavity finesse is given by $f = \lambda/\Delta\lambda$, where λ is the length between successive resonance peaks and $\Delta\lambda$ is the full width at half maximum of a single resonance. Then $Q_L = f\nu$, the product of the finesse and mode number, or about 100. Such a Q factor is quite low compared with the values of 10^4-10^5 typically obtained in Fabry-Perot type resonators at millimeter wavelengths (17). The major factor limiting Q is the relatively large diameter of the coupling holes

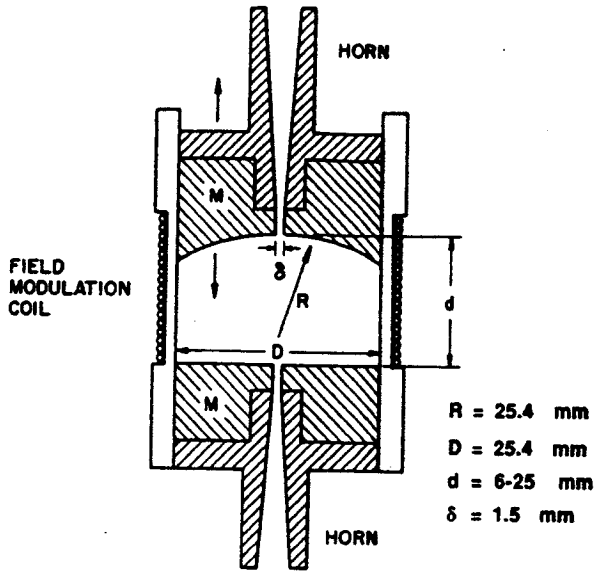

Fig. 3. Fabry-Perot cavity for 250 GHz EPR. M indicates mirror assembly. [From Ref. 9].

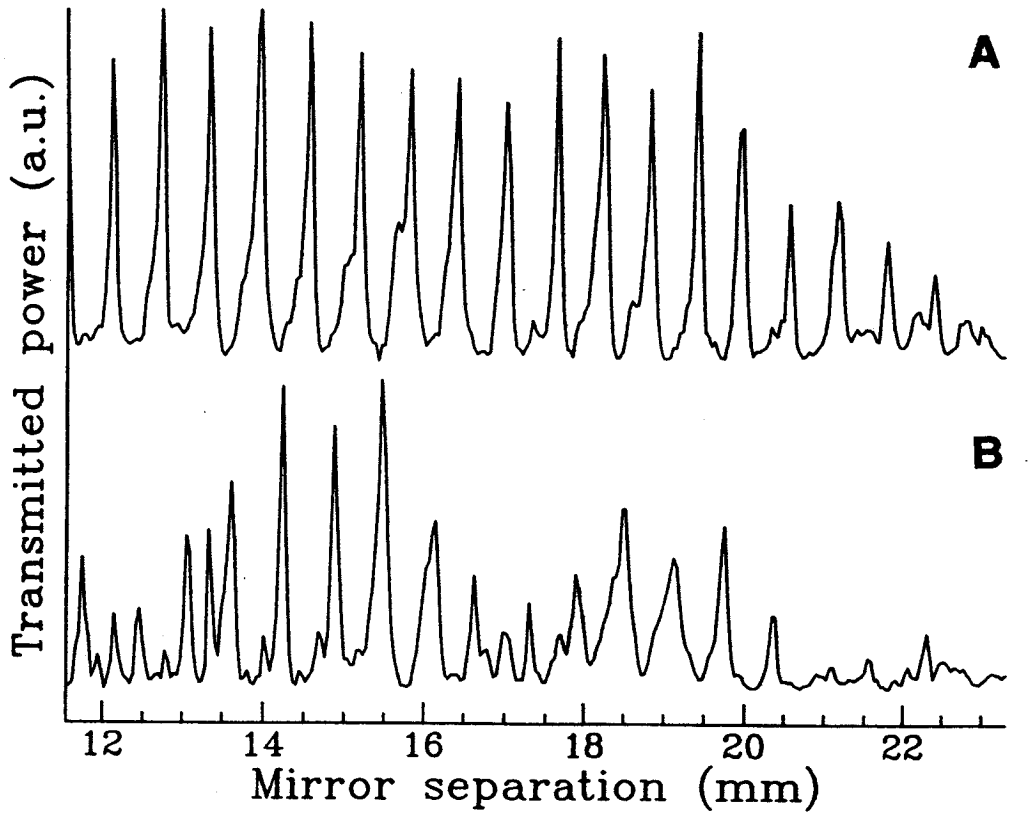

Fig. 4. Transmitted power as a function of mirror separation for the Fabry-Perot cavity under different conditions. (a) Empty teflon sample holder; (b) sample holder plus 50 $\mu\ell$ of toluene (path length 1.0 mm).

compared to the radiation wavelength, leading to a substantially overcoupled cavity. However, a Q of 100 is quite satisfactory for the samples we have examined so far. One advantage of the low Q is that the relatively large width of the cavity resonance peak allows a comfortable tolerance of mechanical misalignment and drift in the cavity dimensions. Thus, cavity tuning is very simple; a resonance is easy to find and maintain at nonambient temperatures.

The flat mirror of the cavity is positioned so that samples placed on it are located within the region of maximum field homogeneity. The field modulation coil is a single solenoid wound around the teflon sleeve (3.2 cm in diameter, 1.25 cm in length, 220 turns of no. 30 magnet wire) and embedded in GE varnish #1202 to reduce mechanical noise at high modulation amplitudes in the 9 T field. The coil is driven by a Wavetek model 197 function generator amplified by a McIntosh audio amplifier, and may be modulated at frequencies from 1 to 100 kHz. The maximum peak-to-peak amplitude currently attainable is only 0.24 mT at the highest frequency; for very broad spectra this limitation somewhat offsets the noise reduction obtained at higher modulation frequencies. At lower frequencies (e.g. 17 kHz) the maximum amplitude is 1.2 mT, which is usually satisfactory for the broad spectra.

2.6 Sample Cells and Temperature Control

The requirement that sample cells be transparent at 1.20 mm places rather strict limitations on the types of materials that can be used in their fabrication. In our initial studies, we have found that polymethylpentene (TPX), teflon, mylar, and Z-cut crystalline quartz (18) have sufficiently low absorbance to be used in sample cells at 250 GHz. However, all these materials have relatively high indices of refraction (e.g., $n \approx 1.4$ for teflon, and $n \approx 2.0$ for crystalline quartz) so that reflection from the sample cell surface is a major concern. It is impractical to machine anti-reflection grooves in the windows of each sample holder; however, reflection can be minimized using techniques adapted from thin-film optics (19).

For millimeter wavelengths, the sample cell wall can be regarded as a "thin film" at the interface of the sample medium with the atmosphere. It can be shown using the Fresnel formulae (19) that the contribution of the film to the reflectance of the interface vanishes when the optical thickness of the film is $m\lambda/2$, where λ is the wavelength of the incident radiation. The only residual effects of the film are a phase shift of $m\pi$ and a slight attenuation by optical absorption. Thus, by adjusting the optical thickness to a convenient integral multiple of $\lambda/2$, many sample cell materials can be made nearly transparent at 1.20 mm.

Fig. 5 shows a sample holder that has proved very successful for hydrocarbons and other low loss solvents such as thermotropic liquid crystals. The holder is designed to maximize the amount of sample within the cavity at the optimal mirror

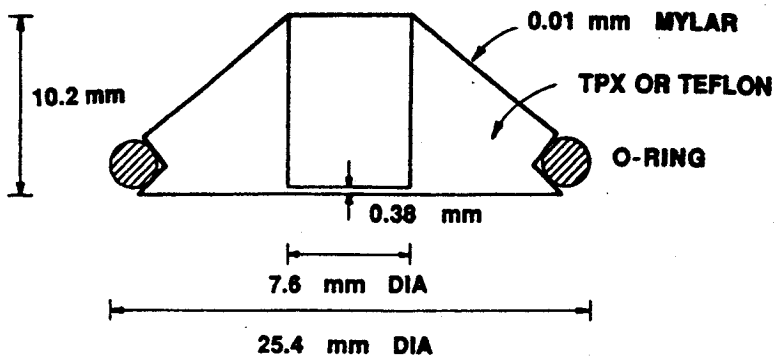

Fig. 5. Sample holder for low-loss liquids in the 249.9 GHz semiconfocal Fabry-Perot cavity. [From Ref. 9].

spacing. The diameter of the sample chamber must be greater than twice the beam diameter at the top of the cell, or at least 5.7 mm, to avoid aperture-limiting the gaussian beam in the cavity. Typical sample volumes are 50-250 $\mu\ell$, which result in a fluid height of several wavelengths.

Samples that require initial degassing to prevent oxygen broadening are degassed on a vacuum line, placed in the sample holder under a nitrogen atmosphere, and then sealed with a 0.01 mm thick mylar film stretched over its top and held in place by an O-ring. During an experiment, the warm bore is swept continuously with nitrogen gas to prevent the dissolution of oxygen into the sample. Nitrogen gas flow also avoids the buildup of frost that occurs when moist room air is trapped in the warm bore by the large diameter of the transmission lens guide tubing. We have found teflon sample cells much more suitable than TPX for working with hydrocarbon solvents and deoxygenated samples.

Initial experiments have also demonstrated Z-cut quartz to a be very useful sample cell material. We estimate its absorbance to be < 0.10 cm^{-1} and the index of refraction to be 2.1 at 1.20 mm (20). The introduction of two 0.28 mm Z-cut quartz windows into the Fabry-Perot cavity has little or no effect on the level or polarization of transmitted power at 250 GHz. The windows are strong enough to permit fabrication of vacuum-sealable sample cells. For our own more specialized purposes, the Z-cut quartz is strong enough be used to prepare well-aligned lipid model membrane samples by a pressure annealing technique (21).

Another material which shows considerable promise for making sample cell windows at 250 GHz is CaF_2, which has very low absorbance at 1.20 mm and a refractive index of about 2.6 (22). Although CaF_2 is very slightly water-soluble, its high strength makes it particularly useful for high pressure applications; furthermore, paramagnetic impurities such as Mn^{2+} may be doped into the cubic CaF_2 lattice sites to serve as field reference markers (23).

Temperature control in the range -170° to +100°C is achieved using a combination of dry nitrogen gas flow through the teflon cavity sleeve and heater resistors located immediately under the bottom mirror. The ambient temperature in the bore is about -20°C; for operation at higher temperatures, the heater resistors are sufficient to provide stable temperature control to within ±1°C, while a slight flow of room temperature nitrogen gas is maintained in the teflon cavity sleeve. For colder temperatures, the nitrogen gas is first passed through a heat exchange coil immersed in a liquid nitrogen bath. Coarse temperature control is obtained by regulating the gas flow, while the heater resistors serve for fine adjustment, again to within ±1°C. Because the tune of the Fabry-Perot cavity is very sensitive to dimensional changes, thorough temperature equilibration of the entire cavity is required before each experiment.

2.7 Millimeter wave detector

The detector (Millitech DXW-4F) is a Schottky diode coupled to a low noise video amplifier with an upper bandwidth corner frequency of about 80 kHz. The detector is the noise-limiting component of the system, producing 1/f noise with a rms voltage amplitude V_n = 50 nV/$\sqrt{Hz}$ at 1 kHz. The responsivity, R_0 of the system is 25 V/mW at 1 kHz and an input power of -20 dBm. At input powers near 0 dBm, at which the detector is operated, the responsivity is at least 12 V/mW over the amplifier bandwidth, giving a noise equivalent power (NEP) of $V_n/R_0 < 4.0\times10^{-9}$ W/$\sqrt{Hz}$. To reduce the 1/f noise of the system, we currently modulate the field at a selection of frequencies from 17 kHz to 80 kHz. The response of the detector is amplified by a Princeton Applied Research HR-8 lock-in amplifier and then is digitized by a Data Translation DT-2801 board in a PC.

3. APPLICATIONS OF 1 MILLIMETER EPR

3.1 Overview

By analogy with NMR, the extension of EPR spectroscopy to fields requiring superconducting magnets and high frequencies has several advantages. Specifically, these are: 1) increased spectral resolution, permitting very accurate determination of the g tensor components, 2) increased sensitivity to molecular motion on the fast time scales of interest for molecular dynamics studies, 3) increased absolute sensitivity in terms of the number of detectable electron spins per unit field.

The ability of the 250 GHz EPR spectrometer to resolve closely spaced g-values recommends it particularly to biological applications. Most biologically relevant free radicals such as electron transport cofactors or nitroxide spin labels have g factors very close to that of the free electron, with very small anisotropies. Moreover, many such radicals have unresolved nuclear hyperfine interactions that produce an EPR linewidth comparable to or larger than the g-

anisotropy. Thus, unlike NMR, where the chemical environment of a spin is usually evident simply from its resonance frequency, conventional EPR of biological radicals often gives little information about their chemical structure or identity. In contrast, 250 GHz EPR can separate radicals with close g-values into different spectral regions, providing a better means of identifying a radical or observing changes in its chemical environment.

Increased spectral resolution also improves sensitivity to molecular orientation. At 250 GHz, g-anisotropy will typically be much more important than hyperfine interactions in determining the spectral width. Thus, different orientations of a given radical can be expected to be better resolved into different regions of the spectrum. This feature presents a powerful means of determining the details of molecular structure in samples where the radicals are macroscopically ordered, such as stretched polymer films, well-aligned lipid bilayers or protein crystals. A much more detailed picture of the orienting potentials and ordering tensors is thus available from high frequency EPR spectroscopy.

An additional advantage of higher frequency is that the range of rotational correlation times that produce slow-motional EPR lineshapes is much higher than that of conventional EPR. Slow-motional spectra from macromolecules are particularly sensitive to details of their motional dynamics. While slow-motional spectra at 9 GHz are observed for rotations with characteristic times longer than a nanosecond, the onset of the slow-motional regime occurs for rotations over an order of magnitude faster at 250 GHz. This permits the 1 mm EPR to reveal details of molecular motion on the time scales typical of biomolecules at physiological temperatures. The sensitivity of the 250 GHz EPR to higher rotational frequencies will be especially useful for identifying ordered and disordered species in biological membranes: motion which appears as rapid averaging at 9 GHz may not be fast enough to lead to spectral averaging at 250 GHz.

An application of 1 millimeter EPR of particular importance for biochemical problems is the study of paramagnetic metal ions, especially those in metalloproteins. Conventional EPR spectroscopy of such systems is quite limited by the large zero field splittings (ZFS) that are generally found in the metal ion. Because the ZFS are usually much larger than the Zeeman interaction at 0.3 T spectrometer fields, the only detectable resonances are the $m_s = +\frac{1}{2} \leftrightarrow -\frac{1}{2}$ transitions that are observable because of time reversal symmetry in ions with an odd number of unpaired electrons. In contrast, the Zeeman interaction at 9 T is comparable to, and in many cases larger than the ZFS of the metal ion. Thus, more EPR transitions should be detectable at 250 GHz, providing much more detailed information about the electronic ground and excited states of the metal ion (24).

3.2 Solid state samples: glasses and polycrystalline powders

The extremely well resolved g-anisotropy of nitroxide spin labels at 250 GHz is most apparent from spectra of randomly oriented, magnetically dilute samples in the rigid limit. Fig. 6 shows derivative spectra of the PD-Tempone spin probe in a frozen glass of 85%/15% glycerol-*d*3/D_2O taken at both 9.5 and 250 GHz. The 9.5 GHz spectrum exhibits the well-known nitroxide rigid limit lineshape with an overall width of 6.78 mT. At 9 GHz, this width is dominated by the ^{14}N hyperfine interaction (typically 3.5 mT); g-anisotropy (typically only 6.0×10^{-3} for nitroxides) only produces a linewidth of ~1 mT at 9.5 GHz. In contrast, the spectrum at 250 GHz reflects mainly g-anisotropy: the x, y, and z orientations of the molecule are resolved into widely separated spectral regions to produce a lineshape resembling those observed at lower fields for paramagnetic species with much larger g-anisotropy. At each of the canonical molecular orientations, three lines corresponding to the ^{14}N hyperfine splitting appear; thus, the hyperfine tensor elements associated with each molecular axis can be independently and accurately measured. The magnetic parameters obtained from a nonlinear least squares fit (25) of the 250 GHz rigid limit spectrum (dotted line in Fig. 6) are summarized in Table I, together with parameters obtained at 9.5 GHz (36). In addition to the elements of the g and A (hyperfine) tensors, the fit at 250 GHz includes an anisotropic T_2 tensor, to account for variation of the intrinsic inhomogeneous linewidth across the spectrum.

A comparison of the 9.5 GHz and 250 GHz results reveals some interesting aspects of the high frequency spectrum. The most noticeable difference between the magnetic parameters measured at 9.5 and 250 GHz are the values of A_x and A_y. Because peaks from the x and y orientations overlap strongly at 9.5 GHz, there is some uncertainty in the values of the A_x and A_y tensor elements obtained by a least squares procedure. In contrast, the g-factor resolution at 250 GHz affords an unambiguous and more precise determination of the A tensor, as well as greater accuracy in the g-tensor.

Another significant feature of the 250 GHz spectrum is the relatively large variation in linewidth with orientation. Whereas the apparent linewidth is less than 0.3 mT at the z orientation, it almost triples towards the x orientation, nearly obscuring the hyperfine structure on the x peak. Two-dimensional electron spin echo experiments have demonstrated that the homogeneous T_2 of PD-Tempone in a frozen glycerol/H_2O glass is nearly constant across the 9 GHz spectrum (26); this is expected to be the case at 250 GHz as well. Anisotropy in the *inhomogeneous* linewidth might be due to unresolved but anisotropic superhyperfine interactions of the deuterons on the radical; however, the isotropic average of the linewidths reported in Table I is much larger than the intrinsic inhomogeneous linewidths observed at 9.5 GHz.

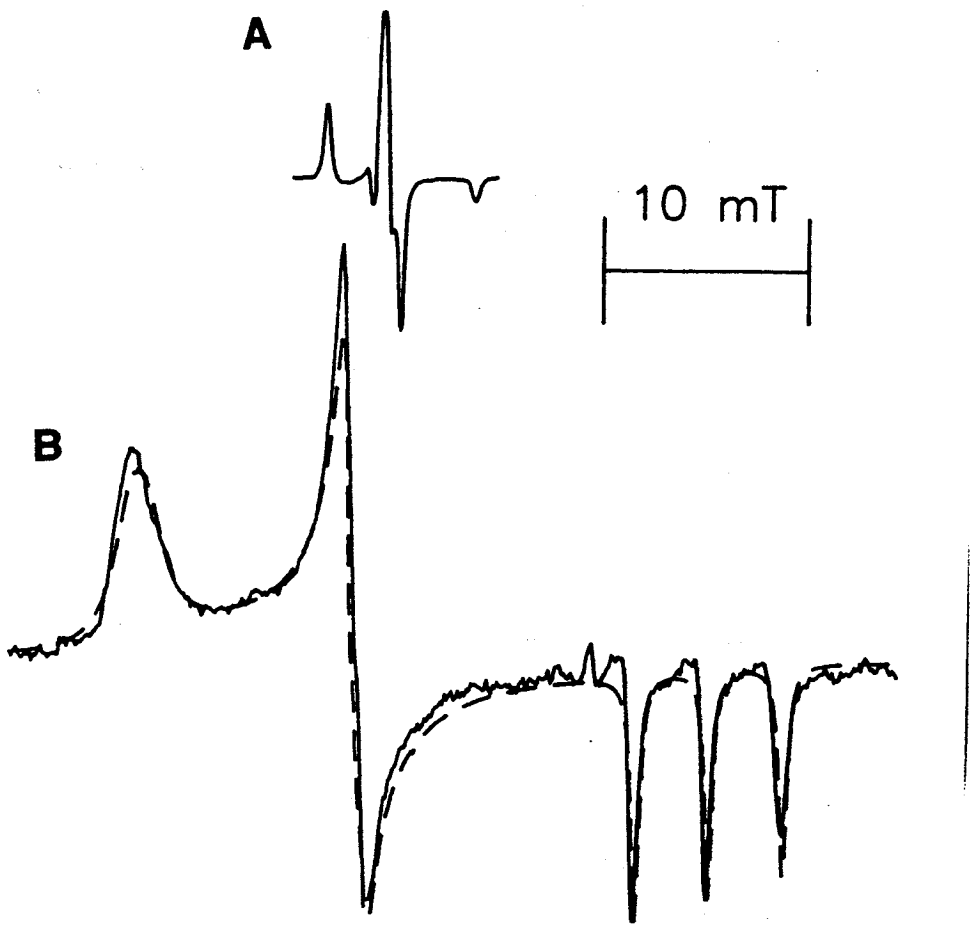

Fig. 6. Rigid limit spectra of 4×10^{-4} M PD-Tempone in a frozen glass of 85%/15% glycerol-*d*3/D_2O (-100°C) taken at (a) 9.5 GHz and (b) 250 GHz.

A more likely explanation of the linewidth variation at 250 GHz is g-strain (27,28), that is, a distribution of g-values arising from inhomogeneity in the local environments of individual spin probes. Since deviations in the effective g from the free electron value $g_e = 2.002322$ are caused by spin-orbit interactions involving the radical's molecular orbitals (29), effective g values will be more sensitive to the local environment the further they are from g_e. Thus, inhomogeneities in local spin environments could produce a distribution in g_x values without significantly affecting g_z, which is consistent with the relative order of the linewidths $T_{2x}^{-1} > T_{2y}^{-1} > T_{2z}^{-1}$ reported in Table I.

The phenomenon of g-strain is well known in the case of paramagnetic transition metals (28), where large spin-orbit coupling terms can produce dramatic variations in g with the crystal field. However, such effects are usually neglected for the small g anisotropies often encountered in organic and biological

Table I. Magnetic parameters of PD-Tempone in 85% glycerol/H_2O (or glycerol-$d3/D_2O$) obtained at 9.5 GHz and 250 GHz.

	9.5 GHz[a] glycerol-d3/D_2O	250 GHz[b] glycerol-d3/D_2O	250 GHz[b] glycerol/H_2O
g_x	2.0084 ± 0.0002	2.00859	2.00860
g_y	2.0060 ± 0.0002	2.00618	2.00622
g_z	2.0022 ± 0.0001	2.00233	2.00233
A_x (mT)	0.55 ± 0.05	0.62	0.66
A_y	0.57 ± 0.05	0.49	0.52
A_z	3.58 ± 0.03	3.62	3.54
T_{2x}^{-1}[c]		0.92	0.96
T_{2y}^{-1}		0.34	0.33
T_{2z}^{-1}		0.23	0.30

(a) Ref. 36.

(b) Uncertainties: g-tensor, approx. 0.00004; A tensor, approx. 0.03 mT.

(c) Expressed as peak-to-peak Lorentzian linewidth in mT.

radicals. The high resolution of g-values at 250 GHz thus provides a sensitive probe of the chemical environment of organic radicals commonly found in biological systems.

Spectra from a rather more complicated solid state sample, a polycrystalline powder of DPPH, are shown in Fig. 7. The 9.5 GHz spectrum is the well known exchange-narrowed result with a derivative linewidth of 0.24 mT, but the one at 250 GHz covers over 7.0 mT with four distinct, broad peaks in the first derivative spectrum. The much smaller peaks are due to individual orientations of microcrystals in the spectrometer field. Because the 1.20 mm beam diameter is small and transmission of the 1.20 mm waves often requires a very thin sample layer, only a limited number of microcrystals can be packed into the active sample volume. We have found that polycrystalline samples must be extremely finely ground to avoid significant deviations from a truly "random" powder pattern.

In most studies of polycrystalline DPPH the g tensor is taken as isotropic, because its asymmetry is so small (30,31,32). Even at higher frequencies (24-36 GHz) the anisotropy is just barely distinguishable; measurements in this frequency range give $g_{\parallel} = 2.0028$ and $g_{\perp} = 2.0039$ (33), in reasonably good agreement with the 5.48 mT splitting of the prominent outer peaks in the 250 GHz spectrum. This demonstrates how small anisotropies in g-tensors virtually unobservable at 9 GHz are dramatically manifested at 250 GHz.

The width of the 250 GHz spectrum is somewhat surprising, since one would expect g-value differences between adjacent molecules to be averaged out by rapid

Heisenberg spin exchange just as the ^{14}N hyperfine tensors are. The exchange interaction has been estimated to be $0.4\text{-}1.0\times10^{11}$ sec^{-1}, compared with $|g_{\parallel}-g_{\perp}|\beta_e B_0/\hbar \approx 10^9$ sec^{-1} at $B_0 = 9$ T (34). However, some features of the 250 GHz spectrum suggest that the exchange may be highly anisotropic. The 5.48 mT splitting shown in Fig. 7 is somewhat narrower than one would anticipate from the g anisotropy of DPPH in dilute solution measured at 2 mm (4). In addition, the spectrum has a faint broad shoulder on the low field side (barely detectable in Fig. 7) suggesting a partial averaging of the g tensor. The additional broad peaks may be due to nearest-neighbor dipolar splittings in the crystal. A useful, detailed interpretation awaits in-depth analysis of the polycrystalline DPPH spectrum; however, our main point here is to emphasize the greatly enhanced spectral sensitivity to both structure and dynamics that is afforded at 250 GHz.

A polycrystalline sample of PD-Tempone similarly produces a single exchange-narrowed line at 9 GHz and a broad spectrum at 250 GHz corresponding to its asymmetric g tensor $g_x = 2.0095$, $g_y = 2.0063$, $g_z = 2.0022$ (35). If the PD-Tempone is prepared in a highly concentrated smear with $CHCl_3$, then even at 250 GHz only a single exchange-narrowed line is observed, as it should be for strong exchange between randomly oriented molecules.

3.3 Magnetically dilute liquid solutions

High frequency EPR can also provide significant new insights into the details of molecular dynamics in the limit of fast motion. At 250 GHz, fast motion corresponds to correlation times $\tau_R < \sim10^{-10}$ sec, typical of many spin probes in liquid phase solution. In this regime, EPR spectra of nitroxide spin probes consist of three Lorentzian lines from the ^{14}N isotropic hyperfine interaction.

Fig. 8 shows spectra obtained at 250 GHz from 5×10^{-4} M PD-Tempone dissolved in deoxygenated toluene-*d*8 at a series of temperatures from -80° to 70°C. Over this temperature range, the rotational correlation time of the spin probe, τ_R, varies by more than an order of magnitude (36). The spectra at 250 GHz are much broader than those obtained at 9 GHz, and the very sharp lines of the 9 GHz spectra change very little with increasing viscosity (36). In fact, only by studying the small differences in linewidth among the hyperfine lines is it possible to estimate the rate of the rotational tumbling that is averaging out the hyperfine-tensor and the g-tensor (10,36,37). The linewidths at 250 GHz are much more dramatically affected by increasing the viscosity. This is illustrated in Fig. 9 where the linewidth of the central peak is plotted as a function of viscosity for both frequencies. The observed trends are consistent with theory (37), which predicts that the g-tensor contribution to the linewidth should depend quadratically on frequency, so that at 250 GHz it is the predominant source of line broadening. Furthermore, the g-tensor contribution is linear in

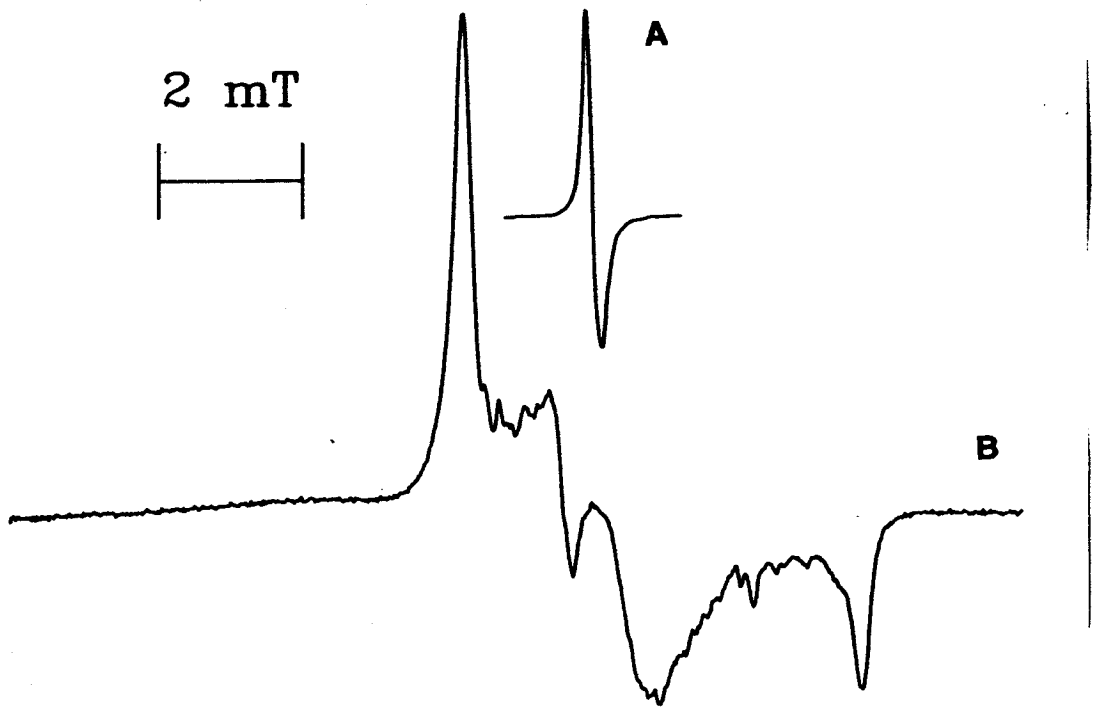

Fig. 7. EPR spectra of polycrystalline DPPH (a) at 9.5 GHz; (b) at 250 GHz at room temperature.

the viscosity for a single solvent, making the 250 GHz linewidths very useful for estimating rotational relaxation times in the motionally narrowed regime.

In contrast, at 9 GHz both spin rotational relaxation and spin exchange make significant contributions to the linewidth that depend inversely on viscosity (10,37). When these effects are combined with the g-tensor contribution, the viscosity dependence of the linewidth is nonlinear and more difficult to interpret. The fast motional spectra at 250 GHz thus provide a means of separating the different contributions to the linewidths. There are additional fundamental questions about the frequency dependence of spin relaxation (10,37) which could be addressed by combining studies at 9 and 250 GHz.

At lower temperatures the EPR spectrum at 250 GHz is no longer in the motionally-narrowed regime, and simple relaxation theory no longer applies. This is evidenced by the large overlap of the hyperfine lines as well as the fact that the width is significantly less than that anticipated from the 9 GHz results. At 250 GHz, this slow-motional regime sets in for values of $\tau_R > \sim 10^{-10}$ sec, which is about an order of magnitude faster than for 9 GHz (35).

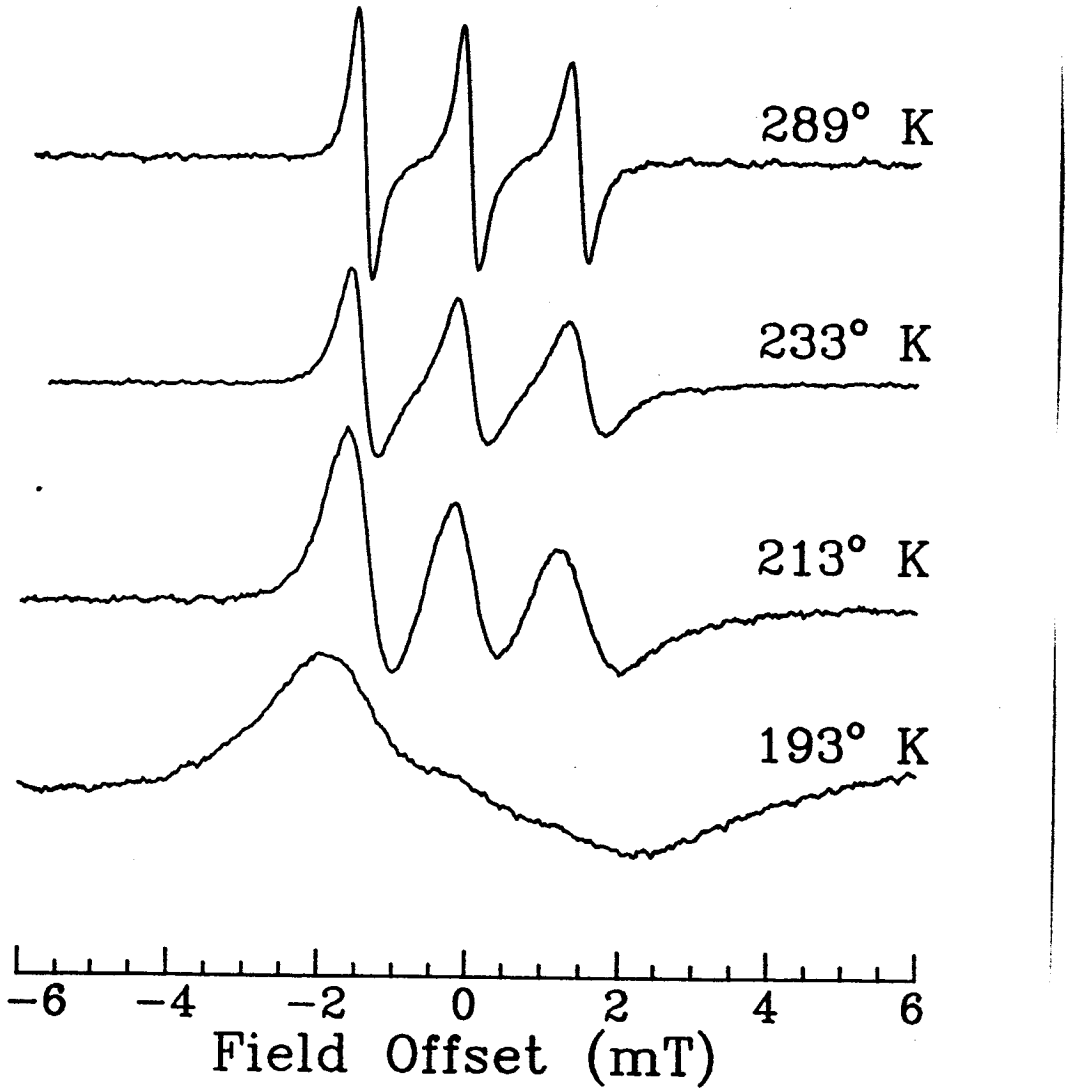

Fig. 8. 250 GHz EPR spectra of 5×10^{-4} M PD-Tempone in toluene-*d*8 at temperatures from -80° to 70°C. All samples are deoxygenated.

3.4 Slow motional spectra: molecular dynamics

250 GHz studies in the slow-motional regime should provide significantly more detailed information about molecular dynamics than is available from motionally narrowed spectra. Fig. 10 demonstrates the sensitivity of the 250 GHz EPR to the motion of two different spin probes at equal concentrations of 5×10^{-4} M in the nematic phase of the thermotropic Phase V liquid crystal (Merck). The upper set of spectra were obtained from the PD-Tempone spin probe, and exhibit the narrow three-line spectrum characteristic of fast molecular motions. At the lowest temperature, the hyperfine lines broaden and start to coalesce as τ_R approaches the slow motional range; however, they remain in the center of the spectrum, indicating nearly isotropic tumbling of the spin probe.

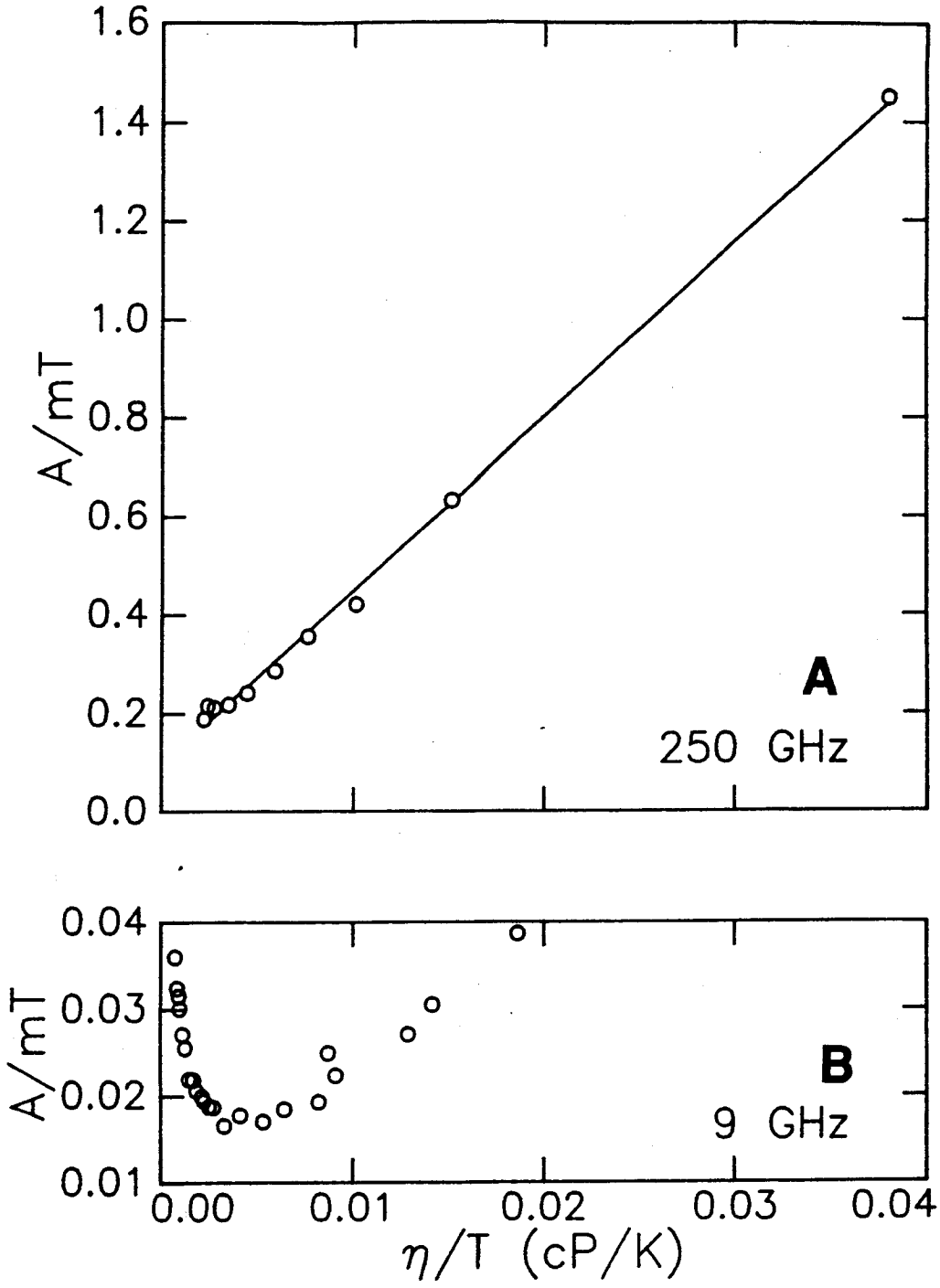

Fig. 9. T_2^{-1} in mT for central hyperfine line of spectra shown in Fig. 8 for 250 GHz and for 9.5 GHz plotted as a function of solvent viscosity, calculated according to reference 36.

The lowest three spectra of Fig. 10 were taken at the same concentration and temperatures using *n*-octylbenzoyl spin label (OBSL), which is a molecular analog for one of the liquid crystal components. In the nematic phase, the probe aligns

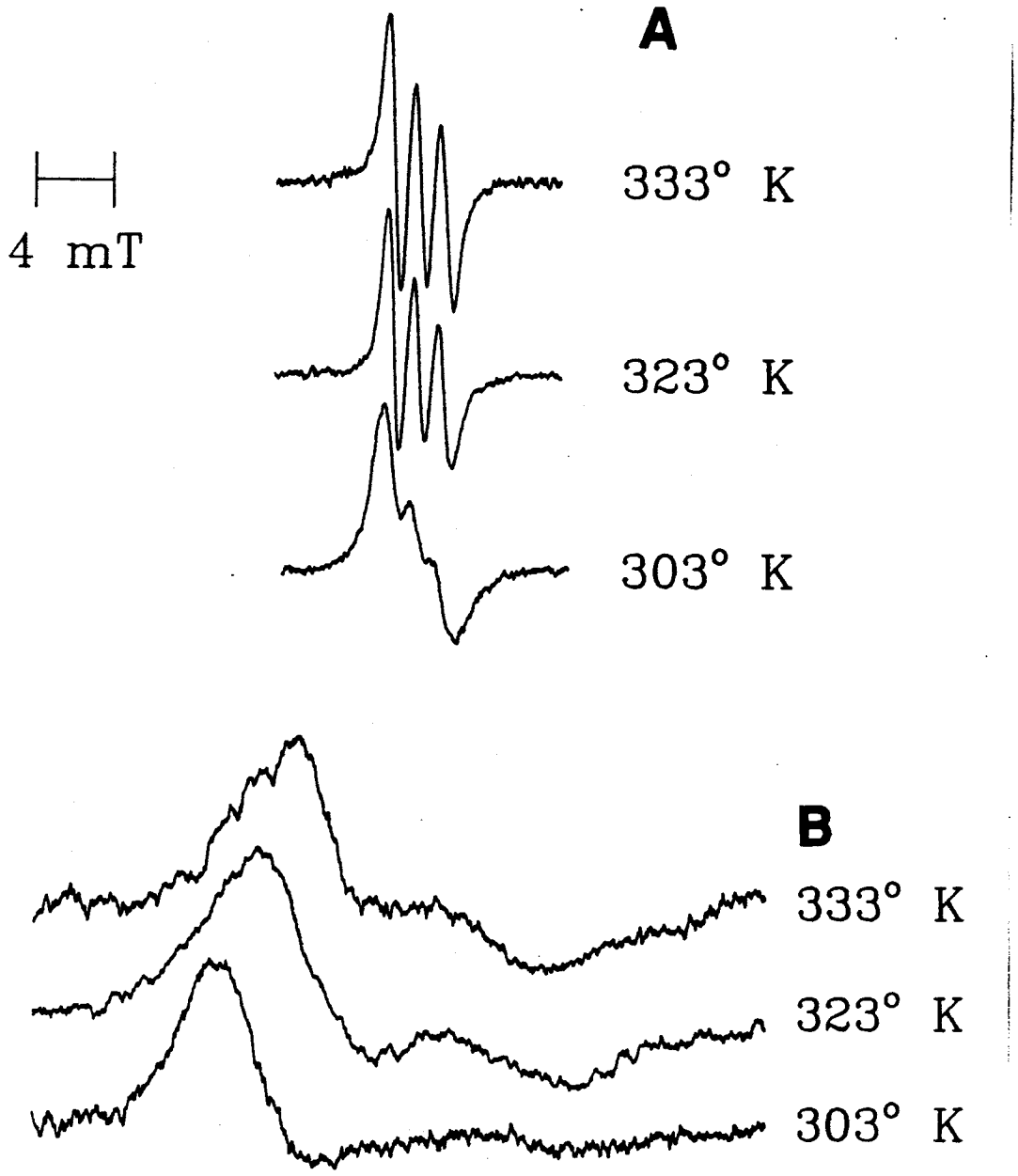

Fig. 10. 250 GHz EPR spectra of (a) 5×10^{-4} M PD-Tempone (b) 5×10^{-4} M OBSL in nematic Phase V liquid crystal (Merck) at a series of temperatures.

so that the N—O bond of the nitroxide radical is nearly parallel to the liquid crystal director. As the much broader spectra indicate, the bulkier OBSL probe undergoes slower rotation than does PD-Tempone. A strong alignment of OBSL in the spectrometer field is also evident from these spectra: they are most intense at field positions near the x orientation of the spin probe, which is with the N—O

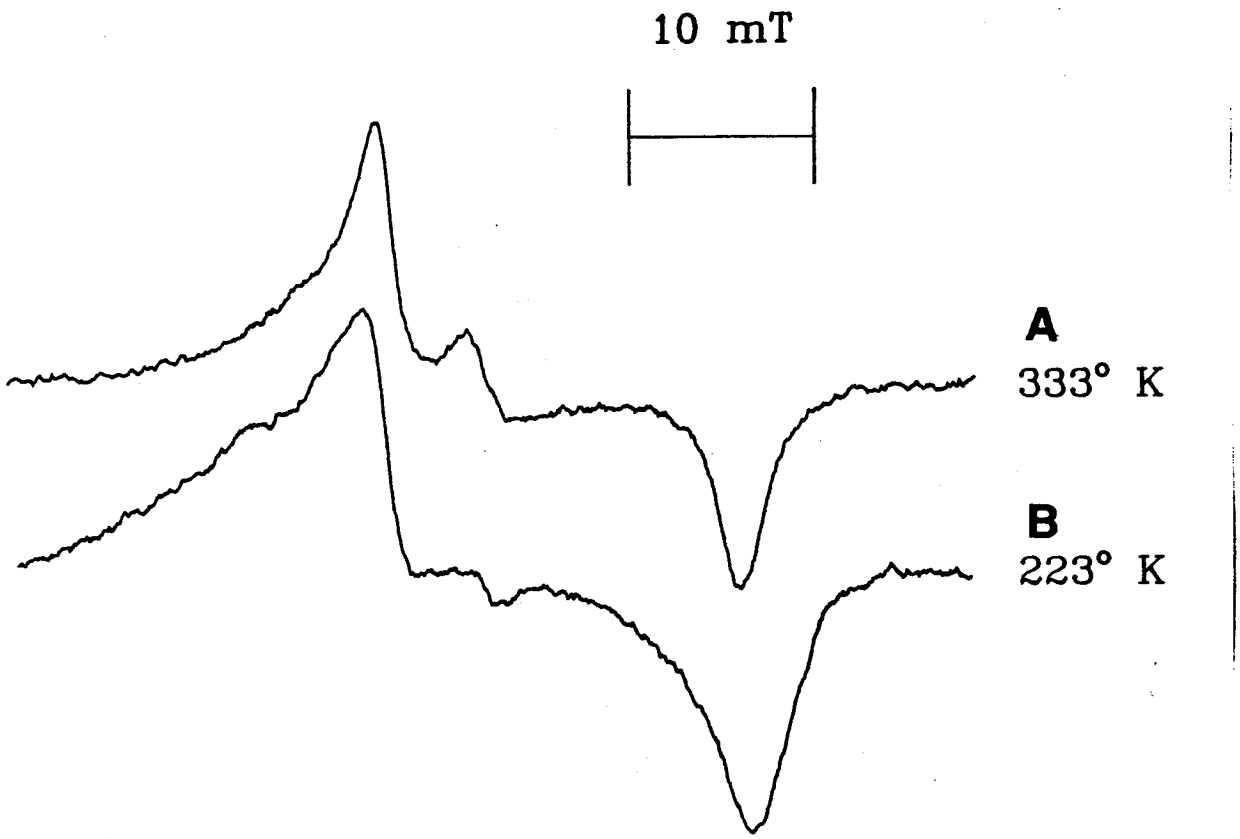

Fig. 11. 250 GHz EPR spectra of CSL (concentration 5.7 mole percent) in an isotropic dispersion of DPPC at (a) 60°C (b) -50° C.

bond, (x axis) along the liquid crystal director and the spectrometer field. When the sample is heated, the intensity shifts towards the center of the spectrum as the spin probe motions become more isotropic. This illustrates how the combined sensitivity of 250 GHz EPR to spin motion and molecular orientation can characterize the directional dependence of the spin interaction.

Studies of slow motion should be particularly useful in the investigation of spin-labeled biological membranes and membrane models. Fig. 11 shows initial results from a sample of the spin label CSL, a doxyl derivative of cholestan-3-one, in a randomly oriented dispersion of the lipid dipalmitoylphosphatidylcholine (DPPC) deposited on a 0.3 mm thickness of Z-cut quartz. These spectra also

maintaining the matching condition $Q_r = Q_u$ for different samples in a high-Q resonator will require that the coupling of the 1.20 mm waves be adjustable.

At conventional microwave frequencies, the most common means of adjusting coupling is by mechanically changing the effective size of the coupling hole. Although a modification of this scheme is practical at 3 mm (42), the fabrication requirements for the coupling elements at 1 mm are too severe. For the present Fabry-Perot cavity, some variability in the coupling may be achieved by substituting flat mirrors with holes of different diameters. The easiest way to fabricate mirrors for this purpose would be to evaporate metal directly onto a sample cell window of quartz or CaF_2.

More continuous adjustability would be possible with a variation on the Bethe coupler that finds use at 2-3 mm (43). This scheme takes advantage of the linear polarization of the radiation incident on the cavity: by placing a short length of rectangular waveguide in front of the cavity and rotating its E-plane relative to the polarization plane of the incident beam, the coupling can be varied monotonically with rotation angle.

A different coupling design is required to operate a reflection cavity in an EPR bridge. The quasi-optical diplexers that are presently available for use in a 1 mm bridge (cf. Section 4.6) require the polarization planes of incident and reflected radiation from the cavity to be orthogonal. Since the Bethe tuning arrangement would result in a variable angle between the polarization planes of incident and reflected radiation, it would be unsuitable for this application. Reflection cavities may therefore require substitution of different iris diameters for coarse tuning; fine-tuning might by achieved by partially inserting a low-loss dielectric in the section of waveguide between the horn to the cavity (44).

The coupling schemes discussed may also require scalar feedhorns to couple the gaussian beam into the cavity instead of the conical antennae currently used. In addition to reducing losses, the feedhorns would match the E and H radiation fields, which would be necessary for any coupling schemes requiring polarization independence, circularly polarized 1 mm waves, or any other superposition of orthogonal polarizations.

Once it is possible to tune the cavity to near critical coupling, it will be necessary to maximize Q_u by minimizing dielectric losses from the sample (45). Lossy samples such as liquid water will require a different holder that can contain the fluid within regions of low E-field in the cavity. For the semiconfocal Fabry-Perot resonator, $E = 0$ at the flat mirror; if a window of optical thickness $m\lambda/2$ is placed on the bottom mirror, E will also vanish near the surfaces of the window. Thus, excessive dielectric losses could be avoided by restricting the liquid layer to within 0.1 mm of the lower mirror or sample cell window. A more practical scheme may be to make the window thickness slightly smaller than $m\lambda/2$, in order to increase the cavity filling factor at some cost in

reflected power. For extremely low spin concentrations, such as might be found in biological samples, alternate "thin layers" of $\lambda/2$ windows and lossy sample could be stacked to maximize the sample volume. An ideal candidate for the windows in this application would be the Z-cut quartz mentioned in Section 2.6.

4.3 Field modulation

Our experience with field modulation in the present spectrometer suggests some simple but useful improvements to the system described in Section 2.5. In EPR spectrometers employing field modulation, coupling between the modulation field and the dc spectrometer field typically produces microphonic vibrations of the modulation coil. Such effects are exaggerated in our 250 GHz spectrometer, where the coil must be placed in a 9 T field. The problems of vibrations are compounded in the present design because the coil is mounted on one of the mirrors. At very high modulation amplitudes, the vibrations modulate the cavity tune, which can produce large baseline offsets in the EPR spectrum. One might expect to avoid such mechanical resonances at higher frequencies; however, the effect does not disappear entirely, presumably because of the large forces involved and the high sensitivity of the cavity to very small dimensional changes. Future designs should mechanically isolate the modulation coil from the Fabry-Perot cavity.

A second difficulty with the current apparatus is the substantial attenuation of the modulation field amplitude at higher frequencies resulting from skin depth effects in the bulk metal of the cavity mirrors. Some mirror heating is also observed at the highest modulation amplitudes as a result of eddy currents in the mirror metal. Such effects will be greatly reduced in the future by constructing the resonator with a minimum amount of metal, preferably only on the surface of each mirror.

4.4 Millimeter wave sources

There are several reasons to increase the source power at 250 GHz. First, increased power would improve the spectrometer sensitivity (cf. Equation 1) at least until power saturation of the EPR transitions sets in. At the present maximum power of 5 mW, we have never observed any indication of spectral saturation. Second, the availability of saturating powers considerably augments the range of experiments that can be performed, e.g. saturation studies of relaxation times. Finally, higher source powers would provide the groundwork for constructing a pulsed spectrometer at 250 GHz.

For many years there has existed a "power gap" in the frequency range 100 GHz to 1 THz. Most of the progress towards higher powers in this frequency range has come from extensions of microwave technology to the near millimeter region. The available sources fall into three categories: electron tubes, FIR lasers, and solid state oscillators. Table II summarizes the output power and FM noise characteristics of different representative sources that may be viable for EPR at

250 GHz. As Table II shows, higher powers are in general only available at a considerable reduction of noise performance. This is not a major concern for the present spectrometer, which is noise-limited by the detector.

The most powerful millimeter wave source available are the electron tube sources, which include reflex klystrons (46), gyrotrons (47), ledatrons (48), backward wave oscillators (BWOs) (49), and extended interaction oscillators (EIOs) (50). Such devices are often bulky, require their own superconducting magnets to operate, and may have short tube lifetimes, especially at the higher frequencies. In addition, they are quite noisy even when phase and frequency locked (49), and some produce output in higher waveguide modes that are difficult to transduce efficiently into a gaussian beam mode.

Lasers also present problems of noise, fragility, bulkiness, and high maintenance overhead. In addition, the lasing transition nearest 250 GHz is a rotation of optically pumped $^{13}CH_3F$, a rather expensive medium. One advantage is that it can provide pulses with peak powers of ~1 MW mm and durations of the order $\leq$ 100 ns (51), which would be useful in time-domain EPR experiments. Other laser systems include the free electron laser (FEL), which is the subject of intense investigation and may become a useable laboratory source in the future.

In contrast, solid state sources, primarily Gunn and IMPATT diodes (52-54), have very low phase noise, and their ease of maintenance and low cost make them very attractive in many applications. A major limitation of solid state sources is the low available output powers; moreover, since they only provide useful

Table II. Performance of selected mm wave sources for use in an EPR spectrometer.

Device	Output Power	Phase Noise dBc/Hz at 100 kHz	Reference
GUNN diode (GaAs)	3 mW	-70	(52)
GUNN diode (InP)	5 mW	-65	(52)
GUNN diode (InP) phase-locked	5 mW	-90	(54)
reflex klystron	8 mW	(a)	(46)
IMPATT diode (280 GHz)	100 mW	-60	(53)
BWO (carcinotron)	500 mW	-80	(49)
EIO (220 GHz)	1 W	(a)	(50)
gyrotron	1 kW	(a)	(47)

(a) Phase noise figure unavailable for this source.

output at fundamental frequencies < ~100 GHz, it is necessary to use frequency doublers or triplers for output at 1 millimeter wavelengths, further reducing the available power and also increasing the phase noise. Because the phase noise of free-running solid state oscillators has approximately a $1/f^2$ frequency dependence between ~10 kHz and ~100 MHz (55), phase-locking considerably improves the noise performance at practical field modulation frequencies (56).

At the modest power levels required to do cw EPR below saturation, the phase-locked, frequency-tripled InP Gunn oscillator used in the present spectrometer provides the best phase noise performance for the available rf power of any available solid state source. The low phase noise at high offset frequencies will also make this source useful as the local oscillator (LO) in a heterodyne detection scheme, so that a relatively noisy but more powerful rf source may be used to irradiate the sample. In principle, a similar heterodyne scheme could also be used with a high-power source in a pulsed spectrometer.

4.5 Detectors

Significant progress in sensitivity at 250 GHz will require a detection scheme with a much lower noise figure than the present direct detection arrangement. Most of the available millimeter wave detectors, such as diode crystals and bolometers, are similar to devices used at conventional EPR frequencies, differing only in the nature of the semiconductor used to make them. The simplest improvement to the present spectrometer would be to use a more sensitive direct detector with the existing transmission cavity; however, more significant noise reduction can be accomplished using coherent detectors (i.e., mixers).

Table III summarizes some performance characteristics for a representative selection of both incoherent and coherent detectors suitable for use in a mm wave EPR spectrometer. The two most useful characteristics for comparing detectors are the detector noise, which limits sensitivity, and the response time, which determines what sort of noise reduction techniques may be used. For incoherent detectors, these characteristics are specified in Table III as noise equivalent power (NEP) and response time constant, τ; for mixers, they are given as noise temperature T_d and intermediate frequency (IF).

As Table III indicates, detector sensitivity is available at a cost in response time or IF bandwidth. At the most sensitive end of the scale are semiconductor bolometers, which perform optimally at or below LHe temperatures. The extreme is the ^{3}He cooled (300 mK) Ge bolometer (57), which is exquisitely sensitive, but has a minimum response time of about 5 ms, severely limiting field modulation frequency and making it particularly sensitive to acoustical noise. The InSb bolometer has the feature that it may be operated as a "hot electron bolometer" (58), taking advantage of the strong dependence of its conductivity on the temperature of its conduction electrons. In contrast, Schottky diode

Table III. Performance of selected mm wave detectors for use in an EPR spectrometer.

Detector	NEP $W/\sqrt{Hz}$	Response Time, τ	Reference
Schottky diode (290 K)	2×10^{-12}	1 nsec	(59)
InSb hot electron bolometer	10^{-13}	100 nsec	(58)
Ge bolometer (^{3}He cooled)	10^{-15}	5 msec	(57)

Mixer	SSB Noise Temperature, T_d	Intermediate Frequency	Reference
Schottky diode (cooled to 20 K)	800 K	1.4 GHz	(62)
InSb hot electron bolometer	360 K	2 MHz	(63)
SIS detector	305 K	1.3 GHz	(64)

detectors are less sensitive, but they provide very fast response times (59), and offer the advantage that they do not require cryogenic cooling. For the present direct detection spectrometer, a hot electron bolometer/pre-amplifier system (60,61) would provide the optimum sensitivity. This device does require cooling, but offers excellent sensitivity at response times that will accommodate useful field modulation frequencies.

As Table III shows, the performance of mm wave detectors with very fast reponse times such as Schottky diodes can be considerably enhanced when they are used as mixers (62). The improvements are mostly due to limitation of the input bandwith, and multiplication of the signal by the local oscillator (LO) frequency. For example, the input bandwidth of a waveguide-mounted incoherent Shottky diode detector is roughly half the center frequency of the waveguide, or 100 GHz for WR-4 waveguide. In comparison, the input bandwidth B of a Schottky diode mixer is about 100 MHz, assuming a typical IF of 1 GHz. The NEP for such a mixer is given approximately by $k_B T_d \sqrt{B} \approx 4\times10^{-16}$ $W/\sqrt{Hz}$, over three orders of magnitude smaller than the NEP for a typical incoherent detector (cf. Table III). The performance of InSb hot electron bolometers may also be considerably improved by using them as mixers (63), although their longer response time results in a somewhat narrow IF bandwidth.

The major difficulty with using a mixer, for example in a heterodyne detection scheme, is that it would considerably complicate spectrometer design. One would require additional quasi-optical elements and two millimeter wave sources for the LO and the rf irradiating the sample. Finally, we note that there has been recent progress (64) towards developing a mm wave detector based upon superconducting effects at cryogenic temperatures (often called superconductor-insulator-superconductor, or SIS detectors), which may prove to be even more sensitive than Ge bolometers, yet have short enough response times to be operated as mixers.

4.6 Quasi-optical bridges and mixers

Ultimately, it will be necessary to employ more sophisticated detection schemes for EPR at 250 GHz. In this section, we consider the millimeter wave analogues of the standard waveguide elements used to construct EPR bridges at conventional wavelengths. The necessary quasi-optical devices are all variations on the Martin-Puplett (MP), or polarizing interferometer (65), shown in Fig. 12, which uses a polarizing wire grid to divide an incident beam of plane-polarized light. The roof-top reflectors m_1 and m_2 rotate the plane of polarization by $\pi/2$, so that both the light initially reflected and the light initially *transmitted* by the grid will be directed towards the output. One of the mirrors is moveable, permitting variation of the relative phase of the two arms and thus the output polarization. Viewed as a rf bridge, the MP interferometer is a four-port device with two inputs (orthogonal polarizations I_1 and I_2 incident on the grid) and two outputs (orthogonal polarizations O_1 and O_2, cf. Fig. 12). Division of input power between the two arms of the interferometer can be controlled by rotating the linear polarization of the source, which can readily be accomplished using a K-mirror (66).

For an EPR bridge, the fixed mirror would be replaced with the Fabry-Perot cavity preceded by a quarter-wave plate (QWP), in order to replace the $\pi/2$ rotation of the roof-top mirror. Plane polarized light incident on the QWP will be converted to a circular polarization before it is coupled into the cavity. Since the polarization maintains its "handedness" upon reflection from the cavity, the QWP converts the reflected radiation back into a planar polarization orthogonal to the incident radiation polarization. One consequence of this arrangement is that the cavity coupling elements, including the waveguide between the coupling horn and the cavity, must have cylindrical symmetry to accommodate the circularly polarized light.

Depending upon the input polarization, the MP interferometer can be operated either as a circulator or as a "magic T" junction. Thus, it will be possible to implement detection methods quite similar to those used at conventional EPR wavelengths; for example, "rf-bucking" to improve the sensitivity of video crystal detectors, balanced mixer arrangements based on the magic T junction, and

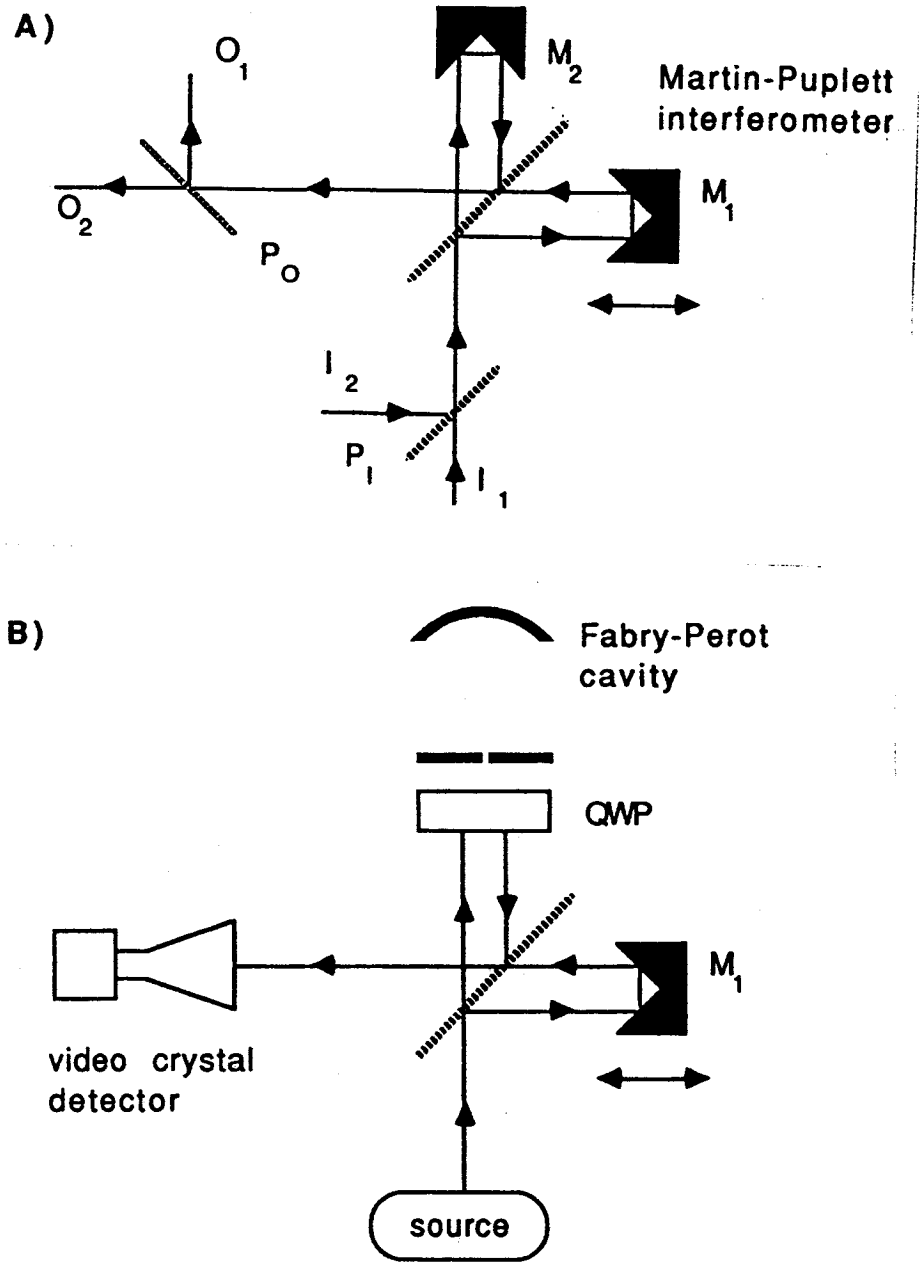

Fig. 12. (a) A Martin-Puplett polarizing interferometer consisting of a polarizing grid and two roof-top mirrors, M_1 and M_2. (b) A quasi-optical EPR bridge (circulator) constructed from a polarizing interferometer.

heterodyne detection using the MP interferometer as an injector for the the local oscillator. Experience with these methods will indicate which is the most advantageous for application at near millimeter wavelengths; however, based on the sensitivity of the various mixers currently available, it would appear that a heterodyne detection scheme should provide the best sensitivity for 1 mm EPR work in the very near future.

5. OUTLOOK

Although EPR spectrometers at near-millimeter wavelengths have been known for a number of years, such spectrometers have often required specialized apparatus or specific types of samples, and thus have not been available for more widespread application to problems of general chemical and biological interest. However, with the advent of readily available sources and quasi-optical technology at millimeter and sub-millimeter wavelengths, we anticipate that high frequency, high resolution EPR will be much more fully utilized in the chemical and biochemical laboratory.

The common availability of high resolution EPR spectroscopy could prove to be a significant asset for EPR studies of biological systems, similar to the enhancements brought to biological NMR work with the introduction of superconducting magnets. Of particular importance for biological studies are the increased spectral resolution for organic free radicals such as electron transport cofactors or nitroxide spin labels, the enhanced sensitivity to molecular dynamics typical of biomolecules at physiological temperatures, and increased absolute sensitivity to the small number of detectable electron spins often found in biological material. The improved sensitivity to molecular orientation is also quite important, since macroscopic order may be imposed on many biological systems using the techniques of stretched polymer films, lipid bilayer alignment, or protein crystallization. Finally, millimeter and sub-millimeter wave EPR can provide a more detailed picture of many biologically relevant metal ions, for which only limited information is available at standard EPR frequencies.

In addition to the advantages of 1 mm EPR demonstrated in this chapter, it may be possible to exploit its potential further by combining it with other spectroscopic methods, similar to methods employed at lower EPR frequencies. The high g-factor resolution afforded at this wavelength particularly suggests 1 mm EPR for techniques that require resolvable magnetic anisotropies such as magneto-photoselection (67). Many interesting chemical species which could not previously be studied by such EPR methods would be approachable at millimeter wavelengths. High g-resolution may also extend the range of samples exhibiting detectable g-strain (27), permitting studies of site selection in a matrix with narrow band laser excitation (68) and the effects of applied electric fields on the g-tensor (69). No doubt further interesting applications of millimeter and sub-millimeter waves will emerge as high-resolution EPR takes its place as a standard laboratory research tool.

ACKNOWLEDGEMENTS

We thank Dave Schneider, Dan Igner, and Dave Bazell for their help during the early stages of spectrometer design, and Eric Smith and Prof. David M. Lee for their advice on the design of the magnet Dewar. Drs. Paul Goldsmith and Ellen Moore of Millitech Corp. are gratefully acknowledged for many useful discussions about quasi-optical devices.

This work was supported by NIH Grant No. GM-25862, NIH National Research Service Award No. 1GM-12924, and NSF Grants Nos. CHE-8703014 and DMR-8616727.

REFERENCES

1 J. Gorcester, G. Millhauser, and J. H. Freed, this volume.
2 S.J. Opella and P. Lu (Eds.), *NMR and Biochemistry*, Marcel Dekker, New York, 1979.
3 A useful text on recent advances in this field is the series by K. J. Button *et al.* (ed.) *Infrared and Millimeter Waves*, Academic Press, New York.
4 O. Ya. Grinberg, A.A. Dubinski, and Ya. S. Lebedev, *Russian Chem. Revs.*, 52 (1983) 850-865.
5 E. V. Lubashevskaya, L. I. Antsiferova, Ya. S. Lebedev, *Teor. Eskp. Khim.* 23 (1987) 46-53.
6 E. Haindl, K. Möbius, and H. Oloff, *Z. Naturforsch.* 40a (1985) 169-172.
7 P. deGroot, P. Janssen, F. Herlach, G. DeVos, and J. Witters, *Intl. J. Infrared Millimeter Waves* 5 (1984) 135-145.
8 F. Herlach (ed.), *Strong and Ultrastrong Magnetic Fields and their Applications*, Vol. 57 in *Topics in Applied Physics*, Springer-Verlag, Berlin, 1985.
9 W. B. Lynch, K. A. Earle, and J. H. Freed, *Rev. Sci. Instr.* 59 (1988) 1345-1351.
10 S.A. Zager and J.H. Freed, *J. Chem. Phys.* 77 (1982) 3344-3375.
11 K.R. Efferson, *Rev. Sci. Instr.* 38 (1967) 1776-1779.
12 For example, see: W.A. Peebles, N.C. Luhmann, Jr., A. Mase, H. Park, and A. Semet, *Rev. Sci. Instrum.* 52 (1981) 360-370.
13 N. R. Erickson, *IEEE Trans.* MTT-29 (1981) 557-561.
14 A. Vickery, Millitech Corp., private communication (1989).
15 P.F. Goldsmith in K. Button (Ed.) *Infrared and Millimeter Waves*, Academic Press, New York, vol. 6 (1982), p. 277.
16 S. B. Cohn, Chap. 14 in: H. Jasik (Ed.) *Antenna Engineering Handbook*, McGraw-Hill, New York, 1961.
17 W. Culshaw, *IRE Trans.* MTT-9 (1961) 135-144.
18 "Z-cut" windows are cut in the basal plane of the quartz crystal, and are available from Valpey Fisher Corp., Hopkinton, Massachusetts.
19 H. A. Macleod, *Thin-Film Optical Filters*, Adam Hilger Ltd., London, 1969, chapter 2.
20 *Handbook of Physics*, American Institute of Physics, Washington, 1972, p. 295.
21 H. Tanaka and J. H. Freed, *J. Phys. Chem.* 88 (1984) 6633-6644.
22 W. Kaiser, W. G. Spitzer, R. H. Kaiser, and L. E. Howarth, *Phys. Rev.* 127 (1962) 1950-1954.
23 B. Bleaney, P. M. Llewellyn, and D. A. Jones, *Phys. Soc. Proc. Ser. B* 69 (1956) 858-860.
24 R. E. Coffman, *J. Phys. Chem.* 79 (1975) 1129-1136.
25 R.H. Crepeau, S. Rananavare, and J. H. Freed, *Proc. 29th Rocky Mtn. Conference*, Denver, CO, Aug. 2-6, 1987.
26 G. L. Millhauser and J. H. Freed, *J. Chem. Phys.* 81 (1984) 37-48.
27 W.R. Hagen, D. O. Hearshen, R.H. Sands, and W.R. Dunham, *J. Mag. Reson.* 61 (1985) 220-232.
28 W. Froncisz and J.S. Hyde, *J. Chem. Phys.* 73 (1980) 3121-3131.

29 C.P. Slichter, *Principles of Magnetic Resonance*, Springer-Verlag, New York, 1980, chap. 10.
30 R.W. Holmberg, R. Livingston, and W.T. Smith, Jr., *J. Chem. Phys.* 33 (1960) 541-546; Y.K. Kim and J.S. Chalmers, *ibid.* 44 (1966) 3591-3597.
31 N.W. Lord and S.M. Blinder, *J. Chem. Phys.* 34 (1961) 1693-1708.
32 J.S. Hyde, R.C. Sneed, Jr., G.H. Rist, *J. Chem. Phys.* 51 (1969) 1404-1416.
33 P.P. Yodzis and W.S. Koski, *J. Chem. Phys.* 38 (1963) 2313-2314; B . M . Kozyrev, Yu V. Yablokov, R.O. Matevosjan, M.A. Ikrina, A.V. Iljasov, Yu.M. Ryshmanov, L.I. Stashkov, and L.F. Shatrukov, *Opt. Spect.* 15 (1963) 340-345.
34 G. Pake and T. Tuttle, *Phys. Rev. Letters* 3, (1959) 423-425.
35 J.H. Freed in: L. J. Berliner (Ed.) *Spin Labeling: Theory and Applications*, Academic, New York, 1976, chapter 3.
36 J. S. Hwang, R. P. Mason, L.-P. Hwang, and J. H. Freed, *J. Phys. Chem.* 79 (1975) 489-511.
37 S.A. Goldman, G.V. Bruno, C.F. Polnaszek, and J.H. Freed, *J. Chem. Phys.* 56 (1972) 716-735; S.A. Goldman, G.V. Bruno, and J.H. Freed, *J. Chem. Phys.* 59 (1973) 3071-3091.
38 C.F. Poole, *Electron Spin Resonance*, Interscience, New York, 1967, p. 546.
39 G. Feher, *Bell System Tech. J.* 36 (1957) 449-484; G.K. Fraenkel in: A. Weisberger (Ed.) *Technique of Organic Chemistry: Physical Methods*, Interscience New York, 1960, vol. I, part IV.
40 P. Goy, in: K. Button (Ed.), *Infrared and Millimeter Waves*, Vol. 8, Academic, New York, 1983, p. 352.
41 G.W. Chantry, *Long Wave Optics*, Academic Press, New York, 1984, vol. 1, p. 68.
42 K. Möbius, personal communication, 1989.
43 R. Clarkson, personal communication, 1989.
44 R. Chedester, Millitech Corp. personal communication, 1989.
45 Note that the dielectric loss term ϵ'' for water is only 5.25 at 250 GHz compared to 32.6 at 9.35 GHz; P.R. Mason, J.B. Hasted, and L. Moore, *Adv. Mol. Relax. Proc.* 6 (1974) 217-233; A.M. Bottreau, J.M. Moreau, J.M. Laurent, and C. Marzat, *J. Chem. Phys.* 62 (1975) 360-365.
46 D. Boilard, Varian Corp. (USA), personal communication, 1989.
47 A. V. Gapanov *et al.*, *Int. J. Electron.*, 51 (1981) 277-287.
48 G. Kantorowicz and P. Palluel, in: K. Button (Ed.), *Infrared and Millimeters Waves*, Vol. 1, Academic, New York, 1979, Ch. 4.
49 A. van Ardenne et al., *Rev. Sci. Instrum.* 57 (1986) 2547-2553.
50 Varian Research Corp. of Canada.
51 M.P. Hacker, Z. Drozdowicz, D.R. Cohn, K. Isobe, and R.J. Temkin, *Phys. Lett.* 57A (1976) 328-330.
52 I. G. Eddison and I. Davies, *Radio Electron. Eng.* 52 (1982) 529-533.
53 H. J. Kuno, in: K. Button (Ed.), *Infrared and Millimeter Waves*, Vol 2., Academic, New York, 1980, Ch. 2.
54 A. Vickery, Millitech. Corp., personal communication, 1989.
55 I. G. Eddison in: K. Button (Ed.) *Infrared and Millimeter Waves*, Vol. 11, Academic, New York, 1984, p. 29.
56 W. P. Robins, *Phase Noise in Signal Sources*, vol. 9 of *IEE Telecommunications*, Peter Peregrinus, London, 1982.
57 H.D. Drew and A.J. Sievers, *Appl. Opt.* 8 (1969) 2067-2071.
58 F. Arams, C. Allen, B. Peyton, and E. Sard, *IEEE Proc.* 54 (1966) 612-622.
59 R. B. Erickson, *Microwaves and RF*, 26 (Dec., 1987) 154-157.
60 J.W. Archer and M.T. Faher, *Microwave, J.* 27 (1984) 135-142.
61 A.T. Wijeratne *et al.*, *Phys. Rev. B* 37 (1988) 615-618.
62 Millitech Corp., 1989.
63 T.G. Phillips, P.J. Huggins, G. Neugebauer, and M.W. Werner, *Astrophys. J.* 217 *(1977) L161.*
64 G.J. Dolan, T.G. Phillips, and D.P. Woody, *Appl. Phys. Lett.* 34 (1979) 347-349.
65 D. H. Martin, in: K. Button (Ed.), *Infrared and Millimeter Waves*, vol. 6, Academic, New York, 1982, chap. 3.
66 P. Goldsmith, Millitech Corp., personal communication, 1989.

67 P. Kottis and R. Lefebvre, *J. Chem. Phys.* 41 (1964) 3660-3661; H.S. Judeikis and S. Siegel, *J. Phys. Chem.* 74 (1970) 1228-1235.
68 R.I. Personov, E.I. Alshits, L.A. Bykovskaya, and B.M. Kharlamov, *JETP* 38 (1973) 912-917.
69 W. B. Mims, *The Linear Electric Field Effect in Paramagnetic Resonance*, Clarendon Press, Oxford, 1976.